Front. Optoelectron. 2017, 10(4): 402–408
DOI 10.1007/s12200-017-0713-9

RESEARCH ARTICLE

Indium tin oxide-free inverted polymer solar cells with ultrathin metal transparent electrodes

Tao YUAN, Zhonghuan CAO, Guoli TU (✉)

Wuhan National Laboratory for Optoelectronics, Huazhong University of Science and Technology, Wuhan 430074, China

Abstract Efficient indium tin oxide (ITO)-free inverted polymer solar cells (PSCs) were fabricated by applying ultrathin metal transparent electrodes as sunlight incident electrodes. Smooth and continuous Ag film of 4 nm thickness was developed through the introduction of a 2 nm Au seed layer. Ultrathin Ag transparent electrode with an average transmittance of up to 80% from 480 to 680 nm and a sheet resistance of 35.4 Ω/sq was obtained through the introduction of a ZnO anti-reflective layer. The ultrathin metal electrode could be directly used as cathode in polymer solar cells without oxygen plasma treatment. ITO-free inverted PSCs obtained a power conversion efficiency (PCE) of 5.2% by utilizing the ultrathin metal transparent electrodes. These results demonstrated a simple method of fabricating ITO-free inverted PSCs.

Keywords polymer solar cells, ultrathin metal transparent electrodes, seed layer, anti-reflective layer

1 Introduction

Polymer solar cells (PSCs) have been extensively studied because of their potential in satisfying the growing consumption of sustainable energy by mankind [1,2]. Considerable effort has been devoted to the commercialization of PSCs [3]. The power conversion efficiency (PCE) of PSCs has improved rapidly over the past several years with the development of new donors [4,5] and acceptors [6], applications of new device structures [7], and interface engineering [8–11]. Moreover, the highest PCE of single-junction PSCs has exceeded 12% [12]. The indium tin oxide (ITO) electrode is the most widely used electrode in PSCs because of its high conductivity, excellent transparency, and compatibility with organic semiconducting materials, but its high cost and poor flexibility limits further application [13]. For satisfying the demand for high conductivity and transparency, low cost, flexibility, and portability, various new electrodes, such as conductive oxides [14], conducting polymers [15], carbon nanotube films [16], graphene films [17], metal nanostructures, and nanowire networks [18,19], have been studied.

In terms of optical transparency and sheet resistance (R_s), metal-based transparent electrodes have become a hot spot because of the highest conductivity of metals compared with materials at room temperature [20]. Ag is widely used due to its high conductivity and low refractive index in the visible region. The thickness of Ag films used as semi-transparent electrodes invariably exceeds 10 nm, and Ag films possess a narrowed transmittance spectrum, decreasing from approximately 70% peak transmittance at 400 nm to below 50% at 800 nm [21]. The poor transmittance of the material does not meet the high transmittance demand as sunlight incident electrode in PSCs. However, when the thickness of Ag film was reduced to several nanometers, the Ag film becomes discontinuous and covered with Ag islands because of "random nucleation" process during thermal evaporation. To overcome this problem, seed layers, such as Au [22], Cu [23], and organic films [21], are introduced as a wetting layer, and smooth, continuous Ag films are obtained with an ultrathin thickness of 3 nm. Promising results have been achieved with the ultrathin Ag film transparent electrodes in organic light-emitting diodes (OLEDs) [24].

In the present paper, we successfully applied an ultrathin Ag transparent electrode as sunlight incident electrode in inverted PSCs. Smooth and continuous Ag film with a thickness of 4 nm was developed through the introduction of 2 nm Au seed layer on glass. With the successive deposition of ZnO anti-reflective layer on top of ultrathin Ag films, we fabricated the ultrathin Ag transparent electrode with an average transmittance of up to 80%

Received March 16, 2017; accepted May 27, 2017

E-mail: tgl@hust.edu.cn

from 480 to 680 nm and a sheet resistance of 35.4 Ω/sq. ITO-free inverted PSCs based on polythieno[3,4-b]thiophene/benzodithiophene:[6,6]-phenyl C_{71}-butyric acid methyl ester (PTB7:$PC_{71}BM$) obtained a PCE of 5.2% by utilizing the ultrathin metal transparent electrode.

2 Experimental

2.1 Materials

PTB7 and $PC_{71}BM$ were purchased from Solarmer Materials, Inc. 1,8-Diiodooctane (98%, DIO) was purchased from Sigma-Aldrich. Molybdenum (VI) oxide (99.95%, MoO_3), and silver shot (99.99%) was purchased from Alfa Aesar. All materials were used as received.

Synthesis of ZnO nanoparticles [25]: a dimethyl sulphoxide (DMSO) solution (30 mL) of zinc acetate hydrate (3 mmol) was mixed with an ethanol solution (10 mL) of tetramethy lammonium hydroxide (TMAH) (5.5 mmol) and stirred for 24 h under ambient conditions. ZnO nanoparticles were precipitated through the addition of ethyl acetate and dispersed in ethanol. A small amount of ethanolamine was introduced to stabilize the nanoparticles.

2.2 Optical simulator

The optical simulator is based on a 1D transfer matrix algorithm [13]. The simulator assumes homogenous media and optically smooth interfaces.

2.3 Device fabrication

Pure glass substrates were cleaned via sonication in deionized water and then baked at 120°C for 120 min. MoO_3/Au/Ag electrodes were deposited on glass by thermal evaporation at a vacuum pressure $< 9 \times 10^{-7}$ torr and an evaporation rate of 0.1 Å/s. For comparison, ITO/glass substrates with a sheet resistance of less than 10 Ω/sq were cleaned via sonication in detergent, deionized water, acetone, and isopropanol for 30 min each, and baked ITO substrates were treated with oxygen plasma for 5 min. ZnO was spin-coated onto the ultrathin metal transparent electrode or ITO substrates and baked at 150°C for 30 min. PTB7:$PC_{71}BM$ (1:1.5 by weight, dissolved in chlorobenzene/1,8-diiodoctane (97:3 vol. %)) were spin-coated on top of the ZnO layer. MoO_3 (10 nm) and Ag electrodes (80 nm) were deposited onto the active layer by thermal evaporation, and the metal electrodes possessed an area of 0.09 cm^2.

2.4 Device characterization

Current density–voltage (J–V) characteristics were recorded by using a computer-controlled Keithley 2400 source meter under an illumination of AM 1.5G 100 mW/cm^2 from Newport solar simulator calibrated by a silicon reference cell.

3 Discussion

In this study, efficient inverted PSCs were constructed by using ultrathin metal transparent electrode as the incident electrode. Conventional ITO-based devices were fabricated for comparison. Ultrathin metal transparent electrode was deposited on glass by simple thermal evaporation. MoO_3 layer was first deposited on the glass substrate, a few nanometer MoO_3 could lead to a more stabilized metal surface on the glass substrate. According to Fig. S1, 3 nm MoO_3 exerted a negligible influence on the transmittance of glass. The average transmittance of glass reaches 90%, and the average transmittance of glass/MoO_3 (3 nm) also remains at 90%.

Atomic force microscopy (AFM) images of glass/MoO_3/Ag (6 nm) and glass/MoO_3/Au (2 nm)/Ag (4 nm) are shown in Fig. 1. The 6 nm Ag film directly deposited on glass/MoO_3 was discontinuous and covered with Ag islands because of random nucleation during thermal evaporation, which was consistent with the results reported by other groups [24,26]. By contrast, a smooth and continuous 4 nm Ag film was developed when 2 nm Au was introduced as a seed layer. Au exhibited higher surface energy than Ag; thus, the introduction of the Au seed layer could develop a wetting layer for subsequent Ag growth, and the agglomerate of Ag atoms is weakened. The root-mean-square (RMS) roughness of MoO_3/Au (2 nm)/Ag (4 nm) film (0.40 nm) is markedly lower than that of MoO_3/Ag (6 nm) (1.07 nm). Moreover, the MoO_3/Au (2 nm)/Ag (4 nm) film exhibits a sheet resistance (R_s) of 40.3 Ω/sq, whereas the MoO_3/Ag (6 nm) film was non-conductive.

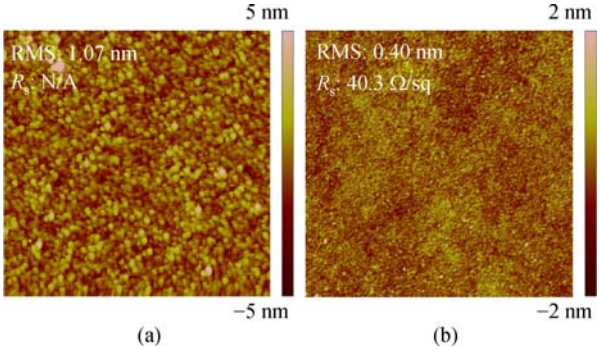

Fig. 1 AFM images of (a) glass/MoO_3/Ag(6 nm) and (b) glass/MoO_3/Au (2 nm)/Ag (4 nm)

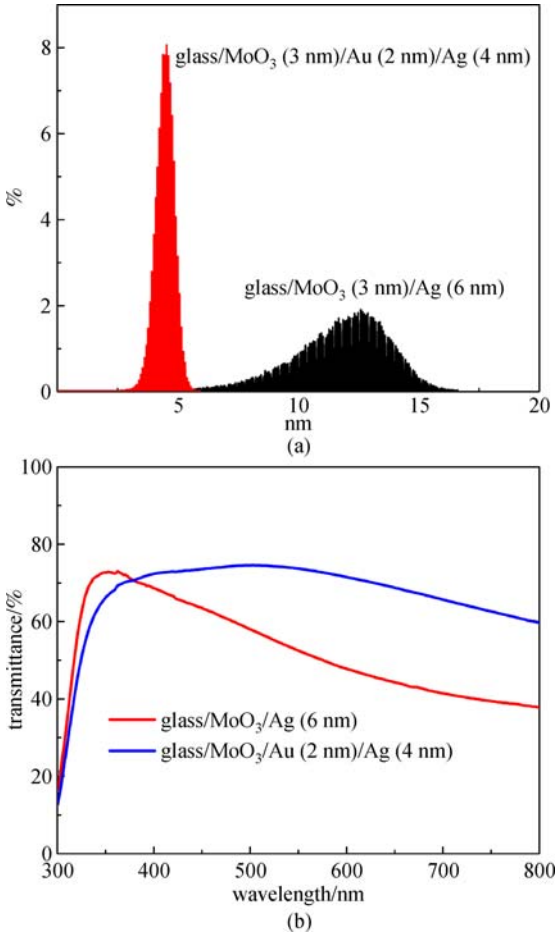

Fig. 2 (a) Histogram of the surface height values for glass/MoO_3/Ag (6 nm) and glass/MoO_3/Au (2 nm)/Ag (4 nm); (b) transmittance of glass/MoO_3/Ag (6 nm) and glass/MoO_3/Au (2 nm)/Ag (4 nm) from 300 to 800 nm

The histograms of the surface height values obtained from the AFM images of MoO_3/Ag (6 nm) and MoO_3/Au (2 nm)/Ag (4 nm) are presented in Fig. 2(a). The figure reveals that the 4 nm Ag film with the 2 nm Au seed layer was more harmonious with an average surface height of approximately 4.75 nm, whereas the 6 nm Ag film without the seed layer was discontinuous with Ag islands at a height of 10 to 15 nm. The isolated Ag islands could increase the undesired absorption of Ag film caused by particle plasmon resonances, which would reduce the transmittance of Ag film. Figure 2(b) presents the transmittance of glass/MoO_3/Ag (6 nm) and glass/MoO_3/Au (2 nm)/Ag (4 nm) from 300 to 800 nm. The transmittance of 4 nm Ag film with Au seed layer is markedly higher than 6 nm Ag film after 400 nm. The average transmittance of glass/MoO_3/Au (2 nm)/Ag (4 nm) from 400 to 750 nm reaches 70%.

The ultrathin metal transparent electrode glass/MoO_3/Au (2 nm)/Ag (4 nm) showed considerably lower transmittance compared with the ITO electrode. For further improvement of the transmittance of ultrathin metal electrode, a ZnO film was introduced to modify the metal electrode. In the present study, ZnO was selected due to its advantages of relatively high electron mobility, environmental stability, high transparency, and easy synthesis in inverted PSCs; moreover, ZnO was widely used as dielectric layer in transparent electrode. The effect of different thicknesses of ZnO film on glass/MoO_3/Au/Ag was modeled, and the results are presented in Fig. 3(a). The figure indicates that the introduction of ZnO could substantially improve the transmittance of the metal electrode with the thickness of ZnO ranging from 10 to 30 nm, and further increase in the thickness of ZnO would reduce the transmittance of metal electrode in the blue light region. The simulated transmittance of metal electrode is superior to the actual measurement results because of ideal assumption in the simulation process. When used as the interface layer in polymer solar cell, ZnO is always approximately 30 nm thick; therefore, we used the ZnO film with a thickness of approximately 30 nm to modify the

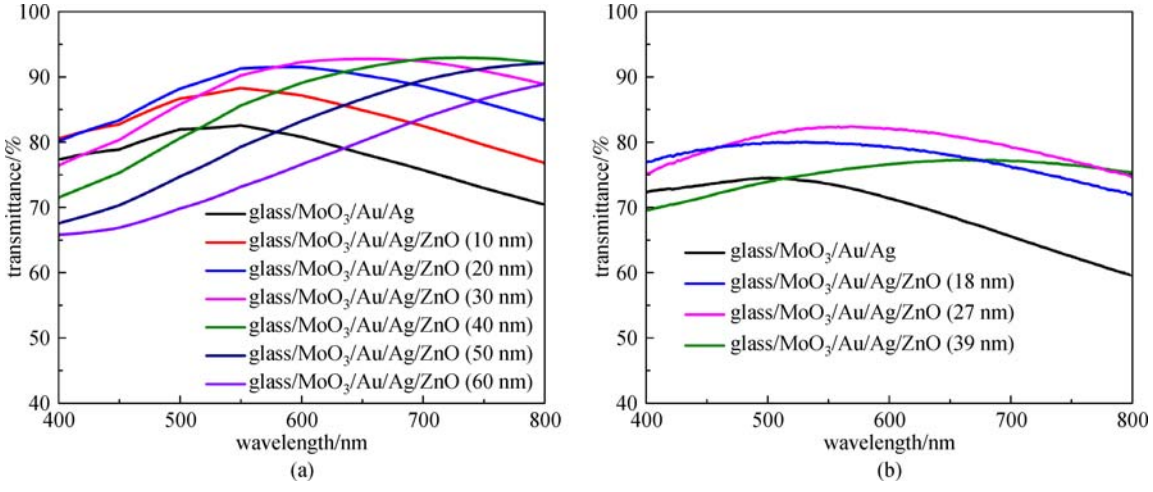

Fig. 3 (a) Modeled and (b) measured transmission of metal electrode modified by ZnO films

metal electrode. The actual transmittance of metal electrode modified by ZnO film is shown in Fig. 3(b). The measured results matched well with the simulated results. The ZnO film could function as an antireflection film, and the transmittance of metal electrode was markedly improved. The average transmittance of glass/MoO_3/Au/Ag modified by 18, 27, and 39 nm ZnO films is summarized in Table 1; the 27 nm ZnO modified metal electrode possessed the highest average transmittance (79.6%). The metal electrode modified by 27 nm ZnO film possessed high transmittance ($>80\%$) from 480 to 680 nm, and the highest transmittance of metal electrode reached 82%. This finding demonstrated that ZnO with a thickness of approximately 30 nm could actually improve the transmittance of metal electrodes.

Figure 4 presents the AFM images of glass/MoO_3/Au/Ag modified by 18, 27, and 39 nm ZnO films. The RMS and R_s of the metal electrodes modified by ZnO films of different thicknesses are summarized in Table 1. With the increase in ZnO thickness, the RMS and R_s of metal electrode both increased. Compared with pure metal electrode, the RMS of 27 nm ZnO modified metal electrode slightly increased to 0.81 nm, whereas the R_s of MoO_3/Au/Ag/ZnO decreased to 35.4 Ω/sq. The 27 nm-thick ZnO film-modified metal electrode possessed the highest transmittance, a smooth surface, and relatively low R_s. Therefore, we selected 27 nm ZnO as the anti-reflective layer to modify the ultrathin metal transparent electrode.

For investigating the effect of ultrathin metal electrode, inverted PSCs were fabricated with a construction of glass/MoO_3/Au/Ag/ZnO/PTB7:$PC_{71}BM$/MoO_3/Ag, and the ultrathin metal electrodes were used as cathode. In addition, the structure of the metal electrodes based devices is illustrated in Fig. 5(a). The chemical structures of PTB7 and $PC_{71}BM$ are shown in Fig. S2. The commonly used devices, that is, glass/ITO/ZnO/PTB7:$PC_{71}BM$/MoO_3/Ag, were also constructed as standard devices. For improved device performance, a good ohmic contact between cathode and the lowest unoccupied molecular orbital (LUMO) energy of $PC_{71}BM$ is required. The work function of MoO_3/Au/Ag/ZnO is obtained from scanning Kelvin probe microscope (SKPM), and highly oriented pyrolytic graphite (HOPG, work function: 4.6 eV) was used as reference. The energy level diagram of metal electrode-based devices is provided in Fig. 5(b). The work function of ZnO modified by metal electrode is 4.3 eV, which approached the LUMO energy of $PC_{71}BM$; thus, the electrons could be well extracted to the metal cathode.

The J–V curves obtained under the illumination of AM 1.5G 100 mW/cm^2 for the PTB7:$PC_{71}BM$ PSCs and using different incident electrodes are presented in Fig. 6(a), and the detailed device parameters, including open circuit voltage (V_{OC}), short-circuit current density (J_{SC}), fill factor (FF), and PCE, are summarized in Table 2. The PTB7:$PC_{71}BM$ PSCs based on ultrathin metal electrode achieved a PCE of 5.20%, with a V_{OC} of 0.71 V, J_{SC} of 11.67 mA/cm^2, and FF of 62.8%. The ITO-based devices achieved a PCE of 7.01%. The V_{OC} of metal electrode based devices was similar to those of ITO-based devices, implying that the ZnO-modified metal electrode could satisfactorily function as cathode in the PSC.

Figure 6(b) presents the transmittance and R_s of different electrodes. The J_{SC} of the PSC is relevant to the absorption intensity of incident sunlight in the active layer, whereas

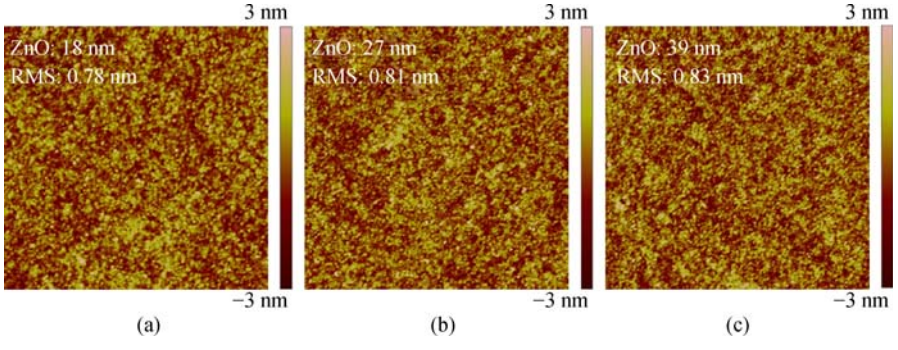

Fig. 4 AFM images of glass/MoO_3/Au/Ag modified by (a) 18, (b) 27, and (c) 39 nm ZnO

Table 1 Average transmittance, RMS, and R_s of glass/MoO_3/Au/Ag modified by 18, 27, and 39 nm ZnO

thickness/nm	transmittance/%	RMS/nm	R_s/(Ω·sq^{-1})
0	69.5	0.40	40.3
18	77.6	0.78	35.3
27	79.6	0.81	35.4
39	75.1	0.83	44.0

Table 2 Detailed devices parameters for the PTB7:$PC_{71}BM$ PSCs with different incident electrodes

cathode	V_{OC}/V	J_{SC}/(mA·cm^{-2})	FF/%	PCE/%
glass/MoO_3/Au/Ag	0.71	11.67	62.8	5.20
ITO	0.71	14.97	66.0	7.01

abundant sunlight is lost in metal electrode-based devices because of the lower transmittance compared with that of the ITO electrode. Therefore, the metal electrode-based devices only achieved a moderate J_{SC}. The AFM images of ITO substrates and ZnO films deposited on ITO substrates are shown in Fig. S3. The ZnO film deposited on metal electrode possessed a more homogenous surface than the film deposited on the ITO electrode. The RMS of MoO_3/Au (2 nm)/Ag (4 nm) film (0.40 nm) is markedly lower than that of the ITO film (4.05 nm). Moreover, the ZnO film deposited on metal electrode (RMS: 0.81 nm) is smoother than ZnO film deposited on ITO substrates (RMS: 1.84 nm), which is beneficial for the contact between active layer and ZnO interface layer. However, the sheet resistance of metal electrode (40.3 Ω/sq) is higher than that of the ITO electrode (9 Ω/sq), negatively influencing FF for higher series resistance in metal electrode-based devices. Thus, the FF of metal electrode-based devices and ITO-based devices was approximate.

4 Conclusions

In conclusion, ultrathin metal transparent electrodes were constructed by simply thermal-evaporating several nanometers of Ag. The introduction of a 2 nm Au seed layer facilitated the development of a continuous Ag film with only 4 nm Ag. Glass/MoO_3 (3 nm)/Au (2 nm)/Ag (4 nm) possessed a more homogenous surface than ITO glass. ZnO film could not only improve the transmittance of metal electrode but also modify the work function. The 27 nm ZnO film-modified metal electrode exhibited an average transmittance of up to 80% from 480 nm to 680 nm, and the ultrathin metal electrode could be directly used as cathode in PSCs without oxygen plasma treatment. A PCE of 5.20% was achieved in PTB7:$PC_{71}BM$-based PSCs. Our results demonstrated a simple method to fabricate ITO-free inverted PSCs.

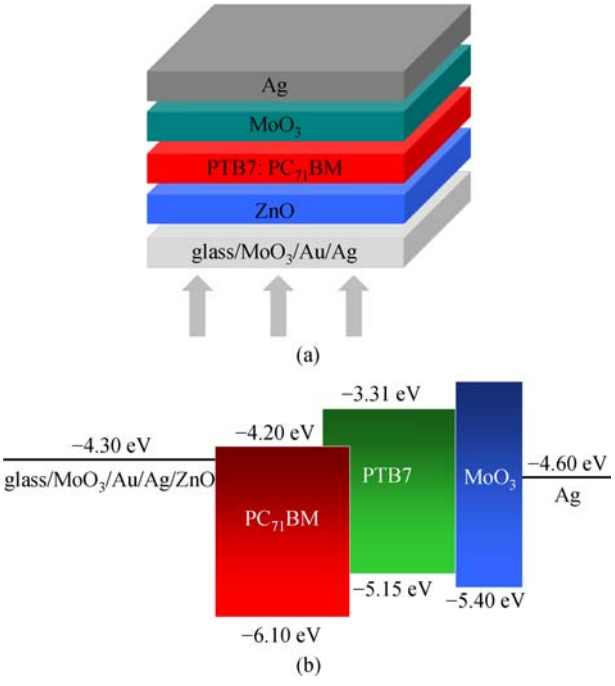

Fig. 5 (a) Device structure and (b) energy level diagram of ultrathin metal electrode-based inverted polymer solar cells

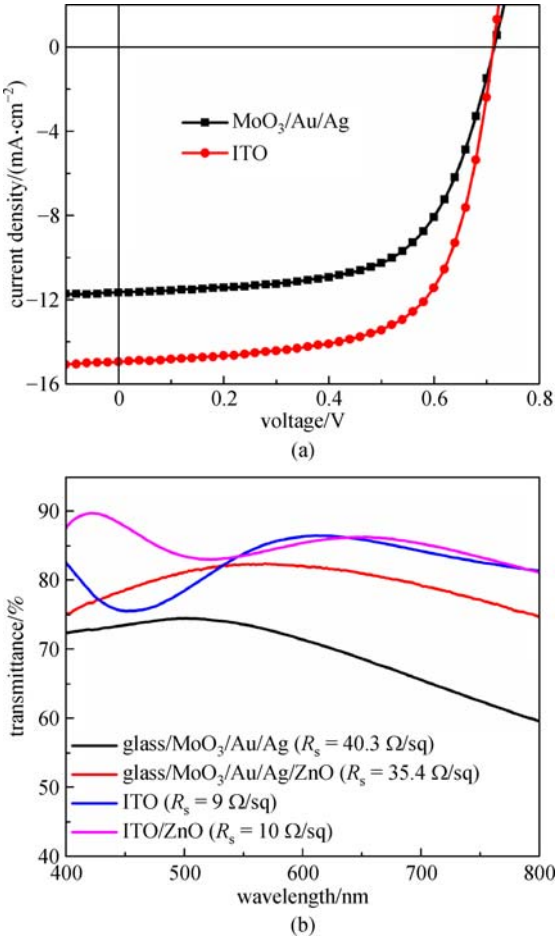

Fig. 6 (a) *J–V* curves obtained under the illumination of AM 1.5G 100 mW/cm^2 for the PTB7:$PC_{71}BM$ PSCs with different incident electrodes; and (b) transmittance and R_s of different electrodes

Acknowledgements This work was financially supported by the National Natural Science Foundation of China (Grant No. 21574049).

Supporting information

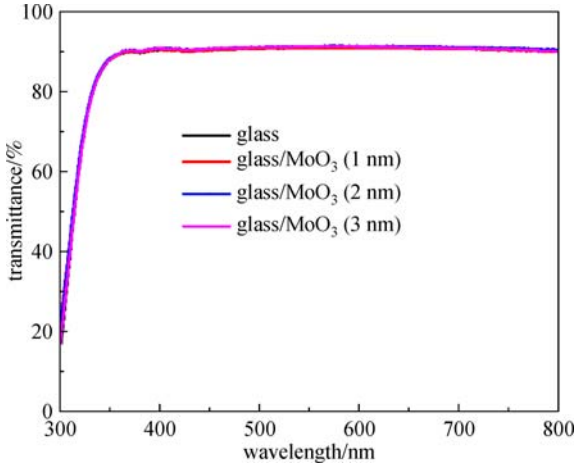

Fig. S1 Transmittance spectra of pure glass and MoO_3 deposited on glass substrates

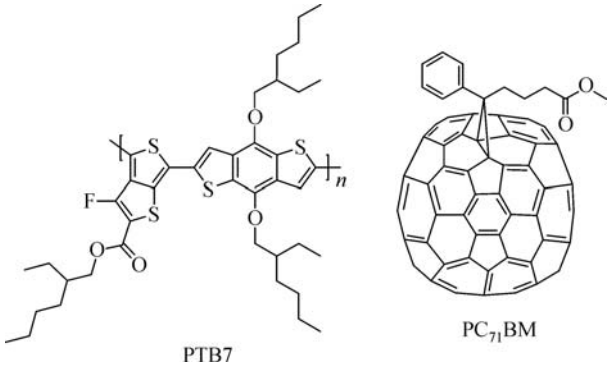

Fig. S2 Chemical structures of PTB7 and $PC_{71}BM$

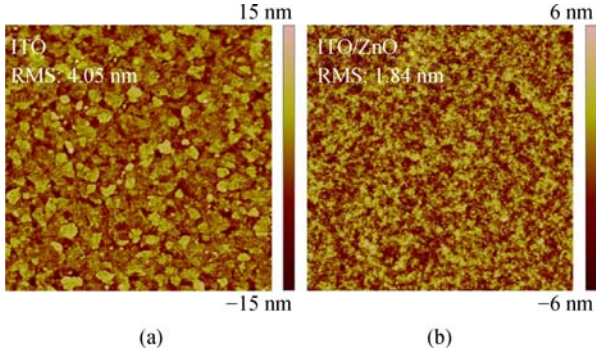

Fig. S3 AFM image of (a) ITO substrate and (b) ZnO film deposited on an ITO substrate

References

1. Li G, Zhu R, Yang Y. Polymer solar cells. Nature Photonics, 2012, 6 (3): 153–161
2. Yu G, Gao J, Hummelen J C, Wudl F, Heeger A J. Polymer photovoltaic cells: enhanced efficiencies via a network of internal donor-acceptor heterojunctions. Science, 1995, 270(5243): 1789–1791
3. Mazzio K A, Luscombe C K. The future of organic photovoltaics. Chemical Society Reviews, 2015, 44(1): 78–90
4. Liu Y, Zhao J, Li Z, Mu C, Ma W, Hu H, Jiang K, Lin H, Ade H, Yan H. Aggregation and morphology control enables multiple cases of high-efficiency polymer solar cells. Nature Communications, 2014, 5: 5293
5. Liang Y, Xu Z, Xia J, Tsai S T, Wu Y, Li G, Ray C, Yu L. For the bright future-bulk heterojunction polymer solar cells with power conversion efficiency of 7.4%. Advanced Materials, 2010, 22(20): E135–E138
6. Zhao W, Qian D, Zhang S, Li S, Inganäs O, Gao F, Hou J. Fullerene-free polymer solar cells with over 11% efficiency and excellent thermal stability. Advanced Materials, 2016, 28(23): 4734–4739
7. Lu L, Kelly M A, You W, Yu L. Status and prospects for ternary organic photovoltaics. Nature Photonics, 2015, 9(8): 491–500
8. Ouyang X H, Peng R X, Ai L, Zhang X Y, Ge Z Y. Efficient polymer solar cells employing a non-conjugated small-molecule electrolyte. Nature Photonics, 2015, 9(8): 520–524
9. Huang L, Chen L, Huang P, Wu F, Tan L, Xiao S, Zhong W, Sun L, Chen Y. Triple dipole effect from self-assembled small-molecules for high performance organic photovoltaics. Advanced Materials, 2016, 28(24): 4852–4860
10. Zhang Z G, Qi B, Jin Z, Chi D, Qi Z, Li Y, Wang J. Perylene diimides: a thickness-insensitive cathode interlayer for high performance polymer solar cells. Energy & Environmental Science, 2014, 7(6): 1966–1973
11. He Z, Zhong C, Su S, Xu M, Wu H, Cao Y. Enhanced power-conversion efficiency in polymer solar cells using an inverted device structure. Nature Photonics, 2012, 6(9): 593–597
12. Li S, Ye L, Zhao W, Zhang S, Mukherjee S, Ade H, Hou J. Energy-level modulation of small-molecule electron acceptors to achieve over 12% efficiency in polymer solar cells. Advanced Materials, 2016, 28(42): 9423–9429
13. Sergeant N P, Hadipour A, Niesen B, Cheyns D, Heremans P, Peumans P, Rand B P. Design of transparent anodes for resonant cavity enhanced light harvesting in organic solar cells. Advanced Materials, 2012, 24(6): 728–732
14. Kumar A, Zhou C. The race to replace tin-doped indium oxide: which material will win? ACS Nano, 2010, 4(1): 11–14
15. Kim N, Kee S, Lee S H, Lee B H, Kahng Y H, Jo Y R, Kim B J, Lee K. Highly conductive PEDOT:PSS nanofibrils induced by solution-processed crystallization. Advanced Materials, 2014, 26(14): 2268–2272
16. Wu Z, Chen Z, Du X, Logan J M, Sippel J, Nikolou M, Kamaras K, Reynolds J R, Tanner D B, Hebard A F, Rinzler A G. Transparent, conductive carbon nanotube films. Science, 2004, 305(5688): 1273–1276

17. Kim K S, Zhao Y, Jang H, Lee S Y, Kim J M, Kim K S, Ahn J H, Kim P, Choi J Y, Hong B H. Large-scale pattern growth of graphene films for stretchable transparent electrodes. Nature, 2009, 457 (7230): 706–710
18. Wu H, Kong D, Ruan Z, Hsu P C, Wang S, Yu Z, Carney T J, Hu L, Fan S, Cui Y. A transparent electrode based on a metal nanotrough network. Nature Nanotechnology, 2013, 8(6): 421–425
19. Garnett E C, Cai W, Cha J J, Mahmood F, Connor S T, Greyson Christoforo M, Cui Y, McGehee M D, Brongersma M L. Self-limited plasmonic welding of silver nanowire junctions. Nature Materials, 2012, 11(3): 241–249
20. Hu L, Wu H, Cui Y. Metal nanogrids, nanowires, and nanofibers for transparent electrodes. MRS Bulletin, 2011, 36(10): 760–765
21. Kang H, Jung S, Jeong S, Kim G, Lee K. Polymer-metal hybrid transparent electrodes for flexible electronics. Nature Communications, 2015, 6: 6503
22. Lenk S, Schwab T, Schubert S, Müller-Meskamp L, Leo K, Gather M C, Reineke S. White organic light-emitting diodes with 4 nm metal electrode. Applied Physics Letters, 2015, 107(16): 163302
23. Formica N, Ghosh D S, Carrilero A, Chen T L, Simpson R E, Pruneri V. Ultrastable and atomically smooth ultrathin silver films grown on a copper seed layer. ACS Applied Materials & Interfaces, 2013, 5(8): 3048–3053
24. Schwab T, Schubert S, Hofmann S, Fröbel M, Fuchs C, Thomschke M, Müller-Meskamp L, Leo K, Gather M C. Highly efficient color stable inverted white top-emitting OLEDs with ultra-thin wetting layer top electrodes. Advanced Optical Materials, 2013, 1(10): 707–713
25. Qian L, Zheng Y, Choudhury K R, Bera D, So F, Xue J, Holloway P H. Electroluminescence from light-emitting polymer/ZnO nanoparticle heterojunctions at sub-bandgap voltages. Nano Today, 2010, 5 (5): 384–389
26. Schubert S, Meiss J, Müller-Meskamp L, Leo K. Improvement of transparent metal top electrodes for organic solar cells by introducing a high surface energy seed layer. Advanced Energy Materials, 2013, 3(4): 438–443

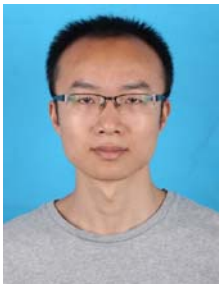

Tao Yuan gained his B.S. degree in the School of Physics and Materials Engineering of Dalian Nationalities University, China, in 2011. He is currently a Ph.D. candidate in optical engineering from Wuhan National Laboratory for Optoelectronics, Huazhong University of Science and Technology. His current research interests include polymer solar cells and transparent conducting electrode.

Zhonghuan Cao received his B.S. degree from the School of Information Engineering of Wuhan University of Technology, China, in 2014. He is studying for a Master's degree in Wuhan National Laboratory for Optoelectronics, Huazhong University of Science and Technology. His current research interests include organic light emitting diodes (OLED) and flexible transparent conducting electrode.

Guoli Tu received his B.S. degree from Jilin University at 1996 and his Ph.D. degree from Changchun Institute of Applied Chemistry, Chinese Academy of Sciences at 2003. He worked at Bergische Universität Wuppertal and University of Cambridge as a postdoctoral researcher from 2004 to 2009. He joined the Wuhan National Laboratory for Optoelectronics, Huazhong University of Science and Technology as a professor in 2009. His group focuses on polymer solar cells and polyimide.